Solar occultation measurement of mesospheric ozone by SAGE III/ISS: Impact of variations along the line of sight caused by photochemistry

Murali Natarajan [1], Robert Damadeo [1], David Flittner [1]

[1] Science Directorate, NASA Langley Research Center, 21 Langley Blvd., Mail Stop 401-B, Hampton, VA 23681, USA.

Correspondence to: Murali Natarajan (murali.natarajan@nasa.gov)

Abstract. Twilight gradients in the concentration of atmospheric species with short photochemical lifetimes influence the transmission data obtained in a solar occultation instrument like the Stratospheric Aerosol and Gas Experiment III aboard the International Space Station (SAGE III/ISS). These photochemically induced changes result in nonlinear asymmetries in the species distribution near the tangent altitude along the line of sight (LOS). The bias introduced by neglecting the effects of twilight variations in the retrieval of mesospheric ozone is the focus of this study. O_3 in the mesosphere exhibits large variations near the terminator during sunrise and sunset based on current understanding of the photochemistry of this altitude region. The algorithm used in the SAGE III/ISS standard retrieval procedure for mesospheric ozone does not include the effects of these gradients. This study illustrates a method for implementing a correction scheme to account for the twilight variations in mesospheric O_3 and gives an estimate of the bias in the standard retrieval. We use the results from a diurnal photochemical model

1

22   conducted at different altitudes to develop a database of ratios of mesospheric O_3 at different

23   solar zenith angles (SZA) around 90° to O_3 at a SZA of 90° for both sunrise and sunset

24   conditions. These ratios are used to scale the O_3 at levels above the tangent altitude for

25   appropriate SZA in the calculation of the optical depth along the LOS. In general, the impact of

26   the corrections due to twilight variations is to increase the contribution of the overlying layers to

27   the optical depth thereby reducing the retrieved O_3 concentration at the tangent altitude. We find

28   that at sunrise the retrieved mesospheric O_3 including the diurnal corrections is lower by more

29   than 30% compared to the archived O_3. We show the results obtained for different latitudes and

30   seasons. In addition, for nearly collocated sunrise and sunset scans, we note that these

31   corrections lead to better qualitative agreement in the sunrise to sunset O_3 ratio with the

32   photochemical model prediction.

33

34   **1   Introduction**

35

36   The solar occultation measurement technique has been the workhorse among various methods

37   used for monitoring the composition of the earth's atmosphere for over 4 decades. This is

38   evidenced by many successful experiments such as SAGE, SAGE II, Halogen Occultation

39   Experiment (HALOE), Atmospheric Trace Molecule Spectroscopy (ATMOS), Atmospheric

40   Chemistry Experiment – Fourier Transform Spectrometer (ACE-FTS), Polar Ozone and Aerosol

41   Measurement (POAM), SAGE III/M3M and SAGE III/ISS. Major advantages of this technique

42   include high signal to noise ratio, high vertical resolution, and long-term accuracy provided by

43   the 'self-calibrating' nature of the instrument operation. Limited global coverage ranks high

44   among the disadvantages of this method. In the occultation experiments, the absorption of solar

45   radiance measured by the instrument as a function of tangent height altitude or pressure is related

46   to the optical depth and hence the abundance of the species along the line of sight (LOS). The

47   bulk of the absorption, in general, occurs around the tangent point because of the exponential

48   decrease in atmospheric density with altitude and due to the slant path determined by the

49   spherical geometry. Algorithms used in standard retrievals assume that the species distribution in

50   atmospheric layers is homogeneous and, therefore, the variation along the LOS is symmetrical

51   around the tangent point location. The column along the LOS is then made up of species

52   concentrations at the tangent altitude and the layers above corresponding to a SZA of 90°. This

53   assumption is quite valid for species such as CH_4, H_2O, and stratospheric O_3 because of their

54   long photochemical lifetimes and the absence of chemically induced diurnal variations. In the

55   case of species with short lifetimes, the sudden changes in the photolysis rates near day/night

56   terminator trigger rapid variations in the concentration as a function of SZA. These variations

57   result in nonlinear asymmetry along the LOS. In this case, the column along the LOS is made up

58   of species concentration at a SZA of 90° at the tangent altitude and those from the layers above

59   at SZA different from 90° on either side of the tangent point.

60

61   The influence of twilight variations in NO and ClO on the interpretation of solar occultation

62   measurements was described by Boughner et al. (1980). Correction factors based on

63   photochemical models, as discussed in the above study, have been routinely applied in the

64   retrievals of stratospheric NO and NO_2 profiles in HALOE (Gordley et al., 1996; Russell et al.,

65   1988) and in ATMOS (Newchurch et al., 1996). Brohede et al. (2007) described the role of

66   diurnal variations in the retrieval of NO_2 from OSIRIS measurements. The algorithm used in the

67   retrieval of NO_2 in SAGE, SAGE II, SAGE III/M3M, and SAGE III/ISS neglects the twilight

68   variations. A recent study of the NO_2 retrieval from SAGE III/ISS by Dubé et al. (2021)

69   describes the importance of considering the diurnal variations along the LOS.

70

71   Mesospheric O_3 is also characterized by short photochemical lifetimes and steep twilight

72   gradients and, therefore, it is a potential candidate species requiring appropriate corrections in a

73   retrieval from solar occultation instruments. Natarajan et al. (2005) noted that the diurnal

74   correction factors used in the retrieval of mesospheric ozone from HALOE (Version 19) needed

75   to be updated. They derived new factors from a diurnal photochemical model of mesospheric

76   ozone and illustrated the impact of the corrections using a small subset of retrieved HALOE

77   mesospheric O_3 profiles. In the present study, we describe the application of similar corrections

78   to the SAGE III/ISS retrieval of mesospheric O_3. Table 1 of the Data Product User's Guide for

79   SAGE III/ISS (2021) lists the release status of mesospheric O_3 data as a Beta version that is yet

80   to be validated, because it is still potentially impacted by spectral stray light within the

81   instrument. Our goal is to quantify the impact of the corrections on the archived data and to see

82   whether the changes can support other known criteria. A description of the mesospheric O_3

83   variations under twilight conditions as calculated with a diurnal photochemical model is given in

84   section 2. The occultation geometry and the diurnal correction factors for mesospheric O_3 are

85   described in section 3. Results from the application of the factors to correct the archived data are

86   discussed in section 4. We also include the results from an approximate retrieval using the

87   archived transmission data with and without diurnal corrections. A comparison of zonally

88   averaged O_3 profiles with scaled data for the same period from the Microwave Limb Sounder

89   (MLS) instrument on Aura satellite is described in the next section. This is followed by a

90   discussion of sunrise to sunset mesospheric O_3 ratios using appropriate collocated scans and a

91 comparison to theoretical values. The final summary section reiterates the importance of

92 corrections for photochemically induced twilight mesospheric O_3 variations in solar occultation

93 retrievals.

94

95 **2   Mesospheric O_3 variations at sunrise/sunset**

96

97 We use a time-dependent, one-dimensional photochemical model to obtain the diurnal variation

98 in mesospheric O_3. A detailed description of the model used in this study is given in Natarajan et

99 al. (2005). This version of the model extends from 56 km to 100 km at 1 km intervals. The

100 photochemical reaction scheme, shown in the Appendix, includes reactions involving species

101 from the Oxygen, Hydrogen, and Nitrogen families. Chlorine and Bromine reactions do not play

102 a significant role in this region of the atmosphere. The adopted chemical rate constant data are

103 from the JPL Publication 19-5 (2020). The diurnal model does not use a family approximation

104 and reactive species O, O_3, N, NO, NO_2, H, OH, HO_2, and H_2O_2 are considered as independent

105 variables. The concentrations of long-lived species are constrained by the results from a two-

106 dimensional chemical transport model (CTM) (Callis et al., 1997). Diffusion coefficients from

107 the CTM are used to parameterize the vertical transport. The diurnal model uses a variable time

108 step, variable order stiff equation solver (Byrne and Hindmarsh, 1975) to integrate the system of

109 species continuity equations. The maximum time step is 600 seconds, and the algorithm

110 automatically reduces the time step to very low values if needed. The model is run for 4 diurnal

111 cycles so that the reactive species reach a steady diurnal behavior, and the results from the fifth

112 cycle are used in the analysis. The model is run for every month at 11 latitudes, corresponding to

113 the latitude nodes of the CTM, from 56.25° N to 56.25° S at an interval of 11.25°.

114

Calculated O_3 diurnal variation in June at the latitude of 11.25° S and at different altitudes of

interest to this work is illustrated in Fig.1. We are restricting our attention to altitudes below 74

km because the SAGE III/ISS O_3 data are noisy in the region above and the quoted uncertainty is

also large. O_3 concentration is shown as a function of time starting at midnight. Nighttime O_3

has a constant value representing the total odd oxygen in the lower mesosphere. A sharp

decrease at sunrise is mainly caused by photolysis of O_3 forming atomic oxygen. The

recombination of atomic oxygen and O_2 quickly balances the loss of O_3 from photolysis. This

reaction is pressure dependent and becomes slower at higher altitudes. The photolysis of O_2

generates additional odd oxygen ($O_X = O + O_3$) and in the morning hours this leads to an increase

in both O_X and O_3. The formation of odd hydrogen species from the reaction of $O(^1D)$ with H_2O

during the day triggers the catalytic destruction of odd oxygen through reactions involving OH.

It is noted that between 50 and 80 km the chemical time constant of O_x is of the order of few

hours and O_x exhibits a diurnal variation caused by the competing production and destruction

reactions. In the early morning there is a net gain of O_X and in the evening, there is net loss of

O_X, which continues even after sunset until atomic oxygen is depleted. The partitioning of Ox

into O and O_3 is mainly controlled by the photolysis of O_3 and the production of O_3 through the

recombination of O and O_2. The large increase in O_3 seen around sunset is mainly due to the

decrease in the photolysis of O_3 and the continuation of the recombination of O and O_2. O_3

reaches a steady value within an hour or so after sunset. The diurnal model extends to 100 km;

however, since the quoted uncertainty above 70 km in the archived SAGE III/ISS O_3 is large, we

will focus on the region below.

136

137   The results of the full diurnal cycle are of general interest about the model simulation. But, with

138   reference to solar occultation measurements, the sharp gradients seen in the O_3 concentration

139   near SZA of 90° are more critical. The significance of the twilight variations to the retrieval of

140   mesospheric O_3 under sunrise/sunset conditions can be understood with the help of the schematic

141   shown in Fig.2. This illustrates the occultation geometry in the plane containing the LOS. The

142   red line denotes the LOS at a tangent altitude of Z_T. Points F and N represent the intersection of

143   the LOS with an atmospheric layer at an altitude of Z shown in green. For a species with little or

144   no twilight variations, the concentrations at the locations F and N are nearly equal to that at the

145   location U, the tangent point at an altitude of Z. In this case, the concentrations at tangent height

146   Z_T can be derived in a straightforward manner from the measured transmission using a retrieval

147   algorithm. However, if the photochemistry causes significant gradients near SZA of 90°, as in

148   the case of mesospheric O_3, the distribution around the tangent point becomes nonlinearly

149   asymmetric because the concentrations at F and N depend on the respective local SZA. This

150   variation must be incorporated in the evaluation of O_3 specific optical depth along the LOS.

151

152   To illustrate the impact of diurnal variations on slant-path column of O_3, we selected a typical

153   event from the SAGE III/ISS data and applied the calculated O_3 variations in the slant-path

154   column evaluation. The required parameters include month, date, event type (sunrise or sunset),

155   tangent altitude, latitude, longitude, spacecraft latitude and longitude. These data are taken from

156   the current Version 5.2 SAGE III/ISS data available from the Atmospheric Sciences Data Center

157   (ASDC) at NASA Langley Research Center. We used the model results for June at 11.25° S

158   latitude to get the O_3 variation at sunrise along the LOS corresponding to different tangent

159   altitudes from 56 to 76 km. The latitude of the chosen SAGE III/ISS measurement is 11.35° S.

160   The O_3 concentration along the LOS for tangent altitude of 64 km is shown as a function of

161   distance along the LOS relative to the tangent point in the left panel of Fig.3. The dotted line

162   corresponds to the O_3 concentration along the LOS when the diurnal variations are neglected and

163   only the values corresponding to 90° SZA from the layers above the tangent altitude are used.

164   The solid line represents the O_3 including the diurnal variations at the respective altitudes. The

165   increased O_3 concentrations on the instrument side of the LOS are readily seen. The ratio of the

166   O_3 column along the LOS with diurnal variations to the column without the diurnal variations is

167   shown as a function of tangent altitude in the panel on the right side. The peak difference of the

168   order of 30% occurs in the altitude range from 61 to 72 km. Underestimation of the partial O_3

169   slant-path column from layers above the tangent altitude in the standard retrieval translates to

170   overestimation of the retrieved O_3 at the tangent altitude. The bias introduced by the neglect of

171   twilight variations can be evaluated with the help of the diurnal model results.

172

173   The technique is to express the O_3 variation as a function of SZA in terms of concentration

174   normalized to O_3 at SZA of 90°. Figure 4 shows the distribution of the ratio $O_3(\theta)/O_3(\theta=90°)$

175   near sunrise as a function of SZA and altitude obtained from the model results for 11.25° S

176   latitude in June. For a given tangent height, the total slant-path O_3 column comprises of partial

177   slant-path columns corresponding to the layers at and above the tangent height. Spherical

178   geometry dictates that the partial pathlength along the LOS is maximum for the layer

179   immediately above the tangent height (i.e., the lowest layer) and decreases dramatically for

180   higher layers. This, combined with decreasing O_3 concentration with height in the lower

181   mesosphere, results in a total slant-path column dominated by contributions from a few layers

182   right above the tangent point. Therefore, only a small range of SZA, say between 86° and 94°,

183   centered at 90° are important. At 62 km the O_3 ratio is less than 1.0 for SZA less than 90° and it

184   increases gradually for SZA greater than 90°. At higher altitudes, the ratio shows a much steeper

185   increase for SZA greater than 92°. The ratio, in some cases, is even slightly larger than 1.0 at

186   SZA less than 90°. From the occultation geometry shown in Fig.2, it is seen that as one moves

187   away from a SZA of 90° along the LOS at any tangent altitude, the corresponding altitude layer

188   of interest moves upwards. Figure 5 illustrates the O_3 twilight ratio as a function of SZA and

189   altitude for sunset conditions for the same latitude and month. The changes in the ratio for sunset

190   condition are smaller and more gradual especially for SZA greater than 90° compared to the

191   sunrise case. It should be recalled that the daytime variation in the odd oxygen concentration in

192   the lower mesosphere impacts the O_3 concentration differently at sunrise and sunset. The

193   differences between the O_3 variations for sunrise and sunset conditions suggest that the effects on

194   the retrievals are different for sunrise and sunset occultations. The twilight O_3 ratios for altitude

195   layers above the tangent altitude can be used to get the O_3 concentration and hence the optical

196   depth along the LOS more accurately.

197

198   Mesospheric O_3 concentrations are influenced by reactions involving HO_x species and therefore

199   the distribution of H_2O used in the model is an important factor. An earlier study with HALOE

200   mesospheric O_3 data (Natarajan et al. 2005) using the results from the same CTM showed that

201   the monthly, zonal mean H_2O distribution from the CTM was in good agreement with the data

202   taken from the UARS reference atmosphere project. Linear trend in mesospheric H_2O and solar

203   cycle response have been addressed in literature (Remsberg et al., 2018; Yue et al., 2019). Yue

204   et al. (2019) report a trend in mesospheric H_2O of the order of 4 to 6% per decade based on the

205   data from the Sounding of the Atmosphere using Broadband Emission Radiometry (SABER) and

206   MLS instruments. Long term variability in H_2O certainly impacts the absolute level of

207   mesospheric O_3. But, for the present study, the factor of importance is the relative variation of

208   O_3 very close to SZA of 90° during sunrise and sunset in the mesosphere. We have done a

209   sensitivity study at 11.25° S in June using the diurnal model with a 25% increase in the H_2O

210   concentration. Figure 6 displays the percent change in the twilight O_3 ratios for sunrise shown in

211   Fig.4. The maximum impact below 74 km is less than 20% and it is very small in the lower

212   regions. The twilight ratio in O_3 is quite robust and small changes in the atmospheric parameters

213   such as temperature and H_2O do not impact this ratio much. The use of this ratio is a valid

214   approximation in correcting the retrieval scheme.

215

216   **3 SAGE III/ISS Mesospheric ozone**

217

218   The Sage III/ISS instrument payload was launched in February 2017 and successfully attached to

219   the ISS. The ISS occupies a low earth orbit at an inclination of 51.64° that provides occultation

220   coverage of low- and mid-latitude regions. Description of the experiment and early validation of

221   the O_3 measurements are given in McCormick et al. (2020) and Wang et al. (2020). More

222   detailed information on the various wavelength channels and data used for retrieving a suite of

223   atmospheric species including mesospheric O_3 are given in SAGE III Algorithm Theoretical

224   Basis Document (ATBD, 2002) and in the SAGE III/ISS Data Products User's Guide Version

225   3.0 (2021) (DPUG). Among the three different O_3 profile measurements made by the instrument,

226   the one based on short wavelengths in the Hartley-Huggins bands refers exclusively to

227   mesospheric O_3. Three Charge-Coupled Device (CCD) pixel groups (PGs 0-2) are assigned to

228   the short wavelengths in the 280-293 nm range, though only one (PG 1 centered at 286 nm) is

229 currently used for the retrieval. According to the DPUG, mesospheric O_3 data have not been

230 fully validated. We also note that the uncertainty in the archived O_3 concentration becomes

231 larger than 10% above 70 km and there are some spurious negative data pointing to uncertainties

232 in the transmission. The present study focusses only on SAGE III/ISS O_3 in the lower

233 mesosphere up to an altitude of 70 km even though the retrieval itself starts at 90 km. The

234 diurnal model described in the previous section extends up to 100 km. We use the Version 5.2

235 transmission and species data obtained from ASDC at NASA LaRC. For each year and month,

236 we have categorized the scans according to event type, sunrise, or sunset. The input data for our

237 analysis include the tangent point latitude and longitude, spacecraft latitude and longitude,

238 vertical profiles of neutral density, mesospheric O_3, and transmission. We use only the

239 transmission data from the science pixel group 1 (PG1), which has a center wavelength of

240 286.124 nm, since the predominant species active in this wavelength region is O_3.

241

242 We have generated a database of O_3 twilight ratios for sunrise and sunset conditions from the

243 diurnal model results. These ratios cover for each month the latitude range from 56.25° N to

244 56.25° S at an interval of 11.25°, SZA from 84° to 96° at 0.5° intervals, and altitudes from 56 to

245 90 km at 0.5 km intervals. Using the input data from each of the SAGE III/ISS occultations and

246 spherical geometry relations, for every tangent altitude we compute the SZA as well as partial

247 pathlengths corresponding to overlying layers. This generates a pathlength matrix like the one

248 used in the standard retrieval. Appropriate O_3 twilight ratios are then obtained by interpolation

249 using the SZA and layer altitude. Multiplication of the standard pathlength matrix by the O_3

250 ratios yields the modified pathlength matrix including the effects of diurnal variations.

251

252   The twilight ratios can either be used to modify the O_3 profiles from the standard retrieval or be

253   incorporated in a new retrieval from measured transmission profile. The first method is like the

254   procedure described by Dubé et al. (2021) for making diurnal corrections to stratospheric NO_2

255   data from SAGE III/ISS. The archived SAGE III/ISS O_3 profile and the standard pathlength

256   matrix are used to recreate the O_3 specific slant optical depth, as shown by the equation

257    $$\tau = \sigma \, S \, n, \hspace{3cm} (1)$$

258   where τ is the O_3 slant optical depth profile, σ is the O_3 cross section corresponding to the center

259   wavelength of PG1, and n is the O_3 profile from the standard retrieval. S represents the

260   pathlength matrix with each row corresponding to a tangent point altitude. This can be written as

261   a triangular matrix because of the geometric symmetry on opposite sides of the tangent point as

262   can be seen from Fig.2. The slant optical depth can then be converted to a O_3 vertical profile

263   corrected for diurnal variations using the modified pathlength matrix described earlier, as shown

264   by the equation

265    $$n_{wd} = (S_{wd})^{-1} \, \tau/\sigma \, = (S_{wd})^{-1} \, S \, n \hspace{2.5cm} (2)$$

266   where S_{wd} is the modified pathlength matrix with diurnal correction and n_{wd} is the corrected O_3

267   profile. Here it is assumed that the O_3 absorption coefficient remains constant along the LOS.

268   This procedure gives a quantitative estimate of the over-prediction by the standard retrieval. The

269   results for a sunrise event on June 14, 2021 (Event ID =2021061438SR) are shown in Fig.7. The

270   left panel displays the O_3 concentration profiles – the solid red line is the archived data from

271   standard retrieval and the solid black line represents the profile after applying the diurnal

272   correction ratios to the pathlength matrix. The percent difference between the standard and the

273   modified profiles is shown by the solid line on the right panel. For this occultation, the difference

274   exceeds 40% above 64 km. This is consistent with the change in O_3 slant column due to the

275   diurnal correction shown in Fig.3. We also note that the retrieval becomes noisy in the upper

276   altitudes as O_3 concentrations reach near detection limits. In the second method, instead of

277   evaluating the slant optical depth using Eq. (1), the archived slant-path transmission data, which

278   corresponds to PG1, is used along with the standard and modified pathlength matrices to retrieve

279   the vertical O_3 profiles. The change in the slant-path transmission corresponding to the science

280   CCD channel PG1 for each tangent altitude below an upper boundary of 90 km is related to the

281   total slant optical depth made up mainly of O_3 absorption and Rayleigh scattering contributions.

282   After removing the Rayleigh scattering part corresponding to the center wavelength of 286.124

283   nm, the slant-path O_3 column can be estimated using the O_3 absorption coefficient at this

284   wavelength taken from Bogumil et al. (2003), which is the same database used in the SAGE

285   retrieval algorithm. The standard and modified pathlength matrices are then used to get the

286   vertical O_3 profiles without and with corrections for diurnal variations respectively. The retrieved

287   O_3 profiles for the sunrise event mentioned earlier are given by the dashed lines on the left panel

288   of Fig.7, the red color denoting the standard retrieval without diurnal corrections and the black

289   color the modified retrieval with diurnal corrections. We have used a very simple algorithm and

290   assumed that the transmission data corresponds to a single wavelength to simplify the

291   calculation. The actual retrieval procedure used for the archived products may have included

292   more refinements. The agreement between results of the two different methods is very good,

293   both for the vertical O_3 profiles and for the percent differences. Results for a sunset event, closer

294   to the above sunrise event in location and within a day (Sunset event ID = 2021061515SS) are

295   shown in Fig.8. The impact of the diurnal correction is much smaller for sunset conditions. The

296   maximum difference between the standard and modified profiles is less than 10%. The two

297   different procedures for incorporating diurnal effects yield very nearly same results.

298

299   We have applied the diurnal corrections following the procedure described above to all the

300   SAGE III/ISS measurements from June 2021, categorized by the event type of sunrise or sunset.

301   Individual O_3 profiles were grouped together in 11 latitude bands, 11.25° wide between 56.25° N

302   and 56.25° S. The percent difference between the standard retrieval profile and the

303   corresponding modified profile, defined as $(O_3/O_{3,\,WD} - 1)\,*100$, was calculated and the mean for

304   each latitude band was evaluated. The subscript WD refers to the retrieval including the diurnal

305   corrections. Figure 9 shows the resulting distribution of the mean, which represents the over-

306   estimation by the standard retrieval, as a function of latitude and altitude. There is a latitudinal

307   dependence with peak values occurring near 64 km and the summer hemisphere showing smaller

308   difference. Values higher than 100% (dark violet region) are seen in the upper altitudes of the

309   winter hemisphere. The O_3 profile has a sharp gradient reaching a very low minimum in winter

310   between and 70 and 80 km. The retrieved data in this region are very noisy and thus sometimes

311   include negative concentrations. The percent difference between the two retrievals also displays

312   a very noisy distribution with large values of both signs. At altitudes above 85 km, the day-night

313   terminator occurs at solar SZA greater than 96° and O_3 variation around 90° is small. The bias in

314   the standard retrieval (not shown) is also small and there is no need for diurnal correction. The

315   distribution of percent differences for sunset measurements is shown in Fig.10. The values are

316   much smaller as discussed earlier, since the diurnal corrections are not significant for sunset. To

317   look at the seasonal dependence of the impact of diurnal corrections on the retrieved O_3, we have

318   repeated the procedure with SAGE III/ISS data from January 2021. Figure 11 displays the results

319   for sunrise conditions. The differences between the standard and modified retrievals are larger

320   again in the winter hemisphere with peak values occurring near 64 km. This agrees qualitatively

14

321   with Fig.11 of Natarajan et al. (2005), which showed the percent difference in retrieved HALOE

322   sunrise O_3 for January 1995 with updated diurnal correction factors compared to the retrieval

323   with HALOE version 19 correction factors. The archived HALOE version 19 retrieval used

324   correction factors from a diurnal calculation at 61 km for all mesospheric tangent altitudes

325   above. Since a partially corrected (version 19) retrieval was used as the basis, the contour levels

326   are negative and smaller in magnitude.

327

328   **4 Comparisons with other measurements**

329

330   It is of interest to see whether the correction to the retrieval of mesospheric ozone described

331   above can be validated by comparisons with other independent measurements. Mesospheric

332   ozone mixing ratios at SZA of 90° during sunrise and sunset have been measured by other solar

333   occultation experiments like HALOE and ACE-FTS. HALOE version 19 retrievals use

334   correction factors based on diurnal model calculation near the stratopause. An update to these

335   correction factors was discussed in Natarajan et al. (2005) but a modified version of the full

336   ozone dataset was not generated. As far as we know, the retrieval scheme of ACE-FTS does not

337   use any correction for twilight variations of mesospheric ozone. It should be emphasized that

338   comparisons with data from other solar occultation experiments do not necessarily provide a

339   robust independent validation of the need to make such corrections to reduce the bias in the

340   measurements.

341

342   MLS aboard the Aura satellite also provides vertical profiles of O_3 extending into the

343   mesosphere. MLS measurements occur twice a day, once in the early afternoon and the other

344   past midnight. Strode et al. (2022) have used the MLS data scaled with factors derived from

345   Goddard Earth Observing System (GEOS) model coupled with the Global Modeling Initiative

346   (GMI) chemistry mechanism for comparisons with SAGE III/ISS O_3 in the stratosphere. We

347   have done similar comparisons for a selected subset of the data in the lower mesosphere using

348   the results from the mesospheric diurnal model described earlier. We limited our attention to the

349   data in altitude range from 56 to 70 km. We used the information provided in the MLS-V5 data

350   quality document (Livesey et al., 2022) to properly screen the O_3 data. The vertical resolution for

351   MLS O_3 varies from 3 to 5.5 km in the lower mesosphere. The reported accuracy varies from 8%

352   at 0.21 hPa to 40% at 0.02 hPa. We used the MLS V-5 O_3 profiles from a 11.25° latitude band

353   centered at 11.25° S from June 13 to June 15 of 2021. The native units of MLS measurements

354   are mixing ratios on pressure levels. We used the MLS temperature and geopotential height data

355   to get O_3 concentrations on an altitude grid. We derived the mean and the standard deviation

356   profiles for both day and night MLS measurements. Results from diurnal model calculations

357   were used to convert MLS day and night measurements to SZA of 90 ° during sunrise and sunset

358   conditions. Figure 12 shows the O_3 concentration at sunrise based on MLS night data by

359   asterisks and that based on MLS day data by diamonds. The horizontal lines represent the

360   standard deviations at different altitudes. We also obtained the mean and standard deviation

361   profiles using SAGE III/ISS data from the same latitude band and period in June 2021 like the

362   selected MLS data. The solid black line in Fig. 12 shows the mean sunrise profile from standard

363   retrieval and the standard deviation is represented by the yellow color band. The dashed black

364   line is the modified retrieval with the green band showing the standard deviation. The twilight

365   corrections to the mesospheric O_3 retrieval brings the profile in better agreement with that

366   derived from MLS day and night data. Above 68 km the MLS day measurements have large

367   variability, and the standard deviation is larger than the mean. Figure 13 shows the comparison

368   of the profiles for sunset conditions. The difference between the modified and the standard

369   retrievals is much smaller for the sunset conditions compared to the sunrise condition. Overall

370   SAGEIII/ISS mesospheric O_3 has a positive bias. The vertical resolution of SAGE III/ISS data is

371   about 0.7 km which is finer than the MLS vertical resolution. We found that the application of

372   the MLS O_3 averaging kernel to smooth the SAGE III/ISS data has a minimum impact on the

373   comparison.

374

375   There have been several ground-based microwave measurements of atmospheric O_3 and its

376   diurnal variations (Connor et al., 1994; Parrish et al., 2014; Sauvageat et al., 2022). The

377   microwave radiometry (MWR) in Switzerland (Sauvageat et al., 2022) provides data temporally

378   overlapping the SAGE III/ISS data. These data are from measurements made at 2 ground stations

379   and they extend into the mesosphere. The vertical resolution of ground based MWR is very

380   coarse in the lower mesosphere, about 17 km (Connor et al., 1994). Therefore SAGE III/ISS O_3

381   data should be convolved with the averaging kernels of MWR prior to comparisons. In addition,

382   MWR provides hourly data and, unless the local measurement time coincides with SZA of 90°

383   during sunrise and sunset, the data must be converted using factors based on diurnal model. We

384   feel that comparison with MWR data is outside the scope of this paper.

385

386   **5 Sunrise to Sunset Ratio**

387

388   Brühl et al. (1996), in their paper on HALOE O_3 channel validation, discussed the sunrise to

389   sunset differences in O_3 around 0.1 hPa (about 64 km). Mesospheric layers are under sunlit

390   conditions even at SZA slightly greater than 90° at dawn and dusk. As explained earlier, the

391   viewing geometry in solar occultation observations leads to an increase in the contribution of

392   overlying layers to the O_3 optical depth because O_3 concentrations corresponding to varying SZA

393   greater than 90° are seen along the LOS. We have noted that the impact is larger during sunrise

394   than sunset measurement. The sunrise to sunset O_3 concentration ratio becomes larger if the

395   diurnal variations along the LOS are not considered in the retrieval. Solar occultation

396   experiments occasionally offer the opportunity to approximately check this ratio as a test of

397   consistency of measurement and agreement with theory. This is possible when sunrise and

398   sunset orbits cross over each other within a reasonably short interval of time and physical

399   proximity. Such near coincidences are quite rare. We selected sunrise/sunset pairs of

400   measurements by SAGE III/ISS having tangent locations within 1.5° latitude, and 15° longitude

401   of each other and separated by a maximum of 36 hours. The effect of advection by the prevailing

402   westerly wind requires that the time and longitude differences are in the correct direction. There

403   are just 10 pairs of sunrise /sunset measurements in June 2021 that satisfy the above criteria, all

404   of them in low latitudes with a mean latitude of 10.46° S at sunrise and 10.27° S at sunset. The

405   mean of the sunrise to sunset ratios of O_3 concentrations from these scans is shown in Fig.14.

406   The solid line corresponding to the standard retrieval shows ratios greater than 1.1 above 60 km.

407   The green color shade represents the standard deviation. The modified retrieval yields a ratio

408   shown by the dashed line decreasing from 1.01 at 60 km to lower values above. The horizontal

409   lines are the standard deviations. The asterisk symbols represent the ratio from the diurnal

410 model. The model value is in good agreement with the ratios from both the standard and

411 modified retrievals near 58 km but above this altitude there is some difference. The variation

412 with altitude in the model ratio is more like that shown by the modified retrieval. The modified

413 retrieval qualitatively reflects the pattern that photochemistry of O_3 suggests in this altitude

414 region. This comparison serves as an independent criterion to highlight the importance of

415 including the LOS twilight variations in the retrieval of mesospheric O_3 in solar occultation

416 measurements. We noticed that very few such pairs of measurements, which satisfied the criteria

417 we have chosen, occurred during other months in SAGE III/ISS data. We have also looked at the

418 latitudinally averaged sunrise and sunset data for June 2021 obtained for generating figures 9 and

419 10. For the latitude band centered at 11.25° S, the sunrise to sunset ratio as a function altitude

420 (not shown) is like Fig.14, which used only collocated data. The small sampling size of the

421 collocated pairs of data and regions of overlapping standard deviations seen in the Fig.14 make

422 this at best an approximate comparison. Other independent measurements are needed to verify

423 the altitude variation of the ratio of sunrise to sunset O_3 concentrations.

424

425 **6 Summary**

426

427 Photochemically induced changes in species concentration at twilight can cause asymmetries in

428 the distribution along the LOS of a solar occultation observation, variations that must be

429 considered in the retrieval algorithm. Prominent among the species that need corrections for

430 twilight variations are NO and NO_2 in the stratosphere and O_3 in the mesosphere. The SAGE

431 III/ISS instrument uses the measurements in the short-wave Hartley-Huggins band to get

432 mesospheric O_3 profiles. The standard retrieval procedure does not consider the LOS variations

433   in O_3 caused by photochemistry. This study describes a procedure to use results from diurnal

434   photochemical model simulations to develop correction factors for different altitudes, latitudes,

435   and months. These factors were used along with the archived SAGE III/ISS mesospheric O_3 data

436   for selected time periods to obtain modified O_3 profiles. For the month of June 2021, it is shown

437   that neglecting the diurnal variations can result in nearly 50% overestimation of O_3 at 64 km at

438   lower latitudes. An approximate retrieval using the transmission data from SAGE III/ISS also

439   indicates similar behavior in the profiles obtained with and without diurnal corrections. The

440   retrievals were repeated for January 2021 to study the seasonal impact. Larger differences are

441   generally seen near 70 km in high latitude winter hemisphere, and this is most likely due to a

442   combination of very low O_3 concentrations, large twilight correction factors, and large

443   uncertainties in the data. The results from this study are in good agreement with those obtained

444   for the retrieval of HALOE mesospheric O_3 data.

445

446   SAGE III/ISS data include a few nearly collocated sunrise and sunset measurements, mostly in

447   the low latitudes and about a day apart. There are 10 pairs of such sunrise and sunset

448   measurements in June 2021. An analysis of the sunrise to sunset ratio profile from these data

449   indicates that the retrievals that include the diurnal variations show qualitatively better agreement
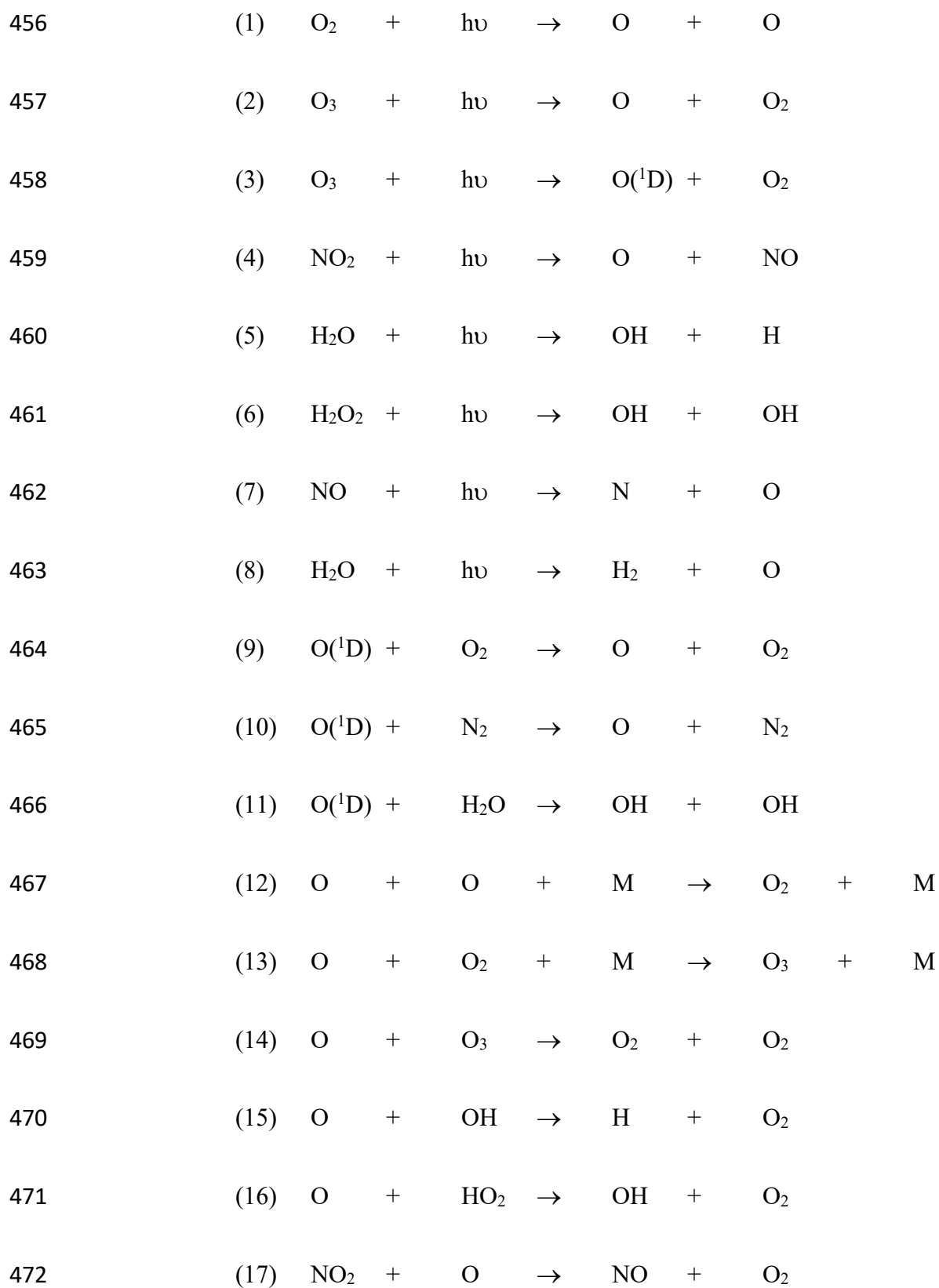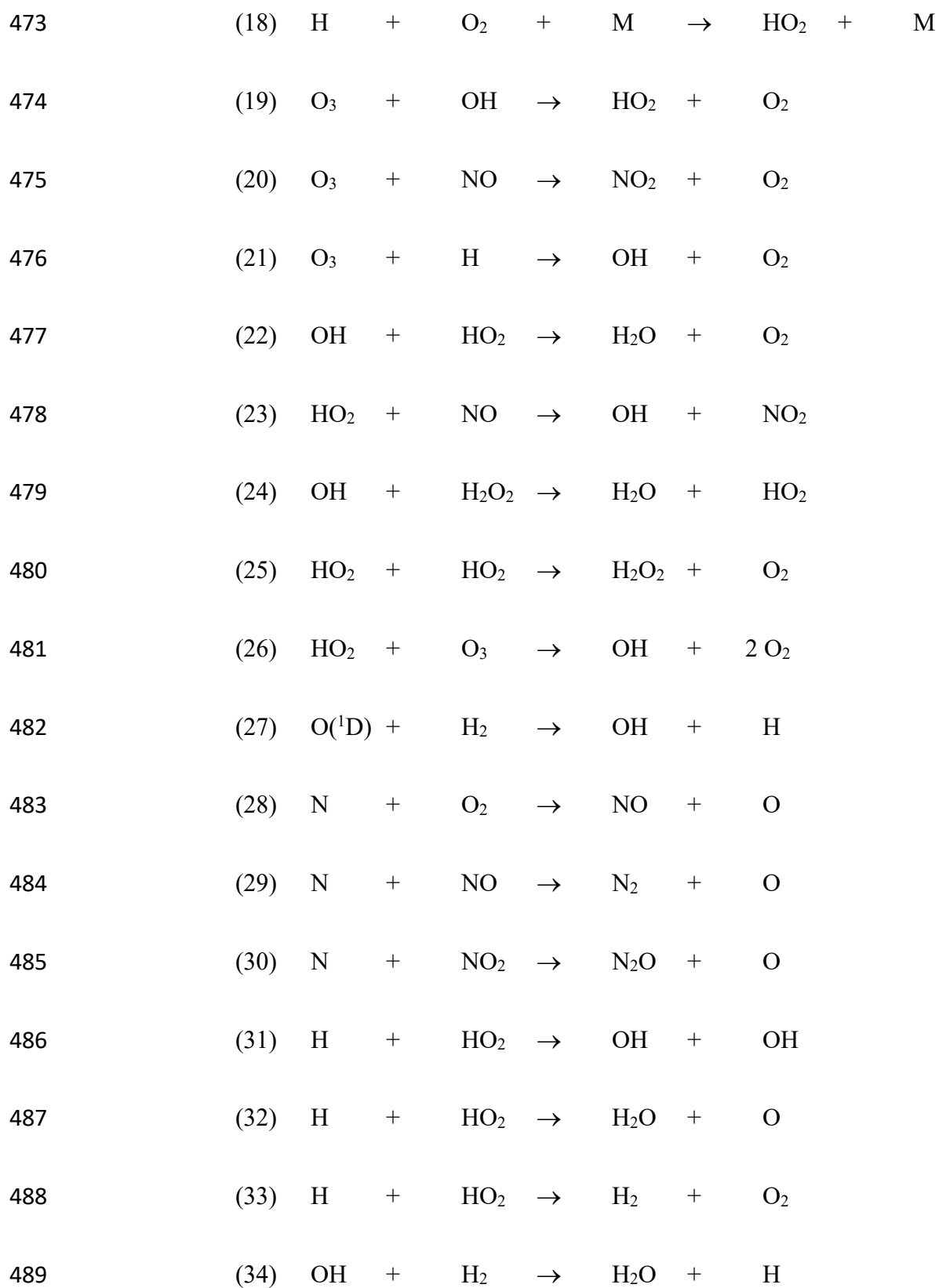
450   with theoretical prediction.

451

452   **Appendix**

453

454   Photochemical reactions considered in the mesospheric diurnal model:

455

456	(1)	O_2	+	hυ	→	O	+	O

456   (1) O_2 +   hυ   →   O   +   O

457   (2) O_3 +   hυ   →   O   + O_2

458   (3) O_3 +   hυ   → $O(^1D)$ + O_2

459   (4) NO_2 +   hυ   →   O   +   NO

460   (5) H_2O +   hυ   →   OH   +   H

461   (6) H_2O_2 +   hυ   →   OH   +   OH

462   (7)   NO   +   hυ   →   N   +   O

463   (8) H_2O +   hυ   → H_2 +   O

464   (9) $O(^1D)$ + O_2 →   O   + O_2

465   (10) $O(^1D)$ + N_2 →   O   + N_2

466   (11) $O(^1D)$ + H_2O →   OH   +   OH

467   (12)   O   +   O   +   M   → O_2 +   M

468   (13)   O   + O_2 +   M   → O_3 +   M

469   (14)   O   + O_3 → O_2 + O_2

470   (15)   O   +   OH   →   H   + O_2

471   (16)   O   + HO_2 →   OH   + O_2

472   (17) NO_2 +   O   →   NO   + O_2

473   (18)   H   + O_2 +   M $\rightarrow$ HO_2 +   M

474   (19) O_3 +   OH $\rightarrow$ HO_2 + O_2

475   (20) O_3 +   NO $\rightarrow$ NO_2 + O_2

476   (21) O_3 +   H $\rightarrow$ OH   + O_2

477   (22)   OH   + HO_2 $\rightarrow$ H_2O + O_2

478   (23) HO_2 +   NO $\rightarrow$ OH   + NO_2

479   (24)   OH   + H_2O_2 $\rightarrow$ H_2O + HO_2

480   (25) HO_2 + HO_2 $\rightarrow$ H_2O_2 + O_2

481   (26) HO_2 + O_3 $\rightarrow$ OH   + $2\,O_2$

482   (27) $O(^1D)$ + H_2 $\rightarrow$ OH   +   H

483   (28)   N   + O_2 $\rightarrow$ NO   +   O

484   (29)   N   +   NO $\rightarrow$ N_2 +   O

485   (30)   N   + NO_2 $\rightarrow$ N_2O +   O

486   (31)   H   + HO_2 $\rightarrow$ OH   +   OH

487   (32)   H   + HO_2 $\rightarrow$ H_2O +   O

488   (33)   H   + HO_2 $\rightarrow$ H_2 + O_2

489   (34)   OH   + H_2 $\rightarrow$ H_2O +   H

Data Availability

SAGE III/ISS version 5.2 data is available from https://asdc.larc.nasa.gov/project/SAGE%20III-ISS/g3bssp_52. MLS O_3 data are available from https://disc.gsfc.nasa.gov/. O_3 twilight ratios used in this study are available from the author. They can also be obtained from any diurnal photochemical model of the mesosphere.

Author Contribution

MN conducted the photochemical model calculations, SAGE III/ISS O_3 retrievals, and the analyses described in the study, and he wrote the manuscript. RD and DF provided information and guidance on the use of SAGE III/ISS mesospheric O_3 data as well as comments on the manuscript.

Competing Interests

The authors declare that there is no competing interest for this study.

References

Bogumil, K., Orphal, J., Homann, S., Voigt, P., Spietz, O., Fleischmann, A., Vogel, M.,

Hartmann, H., Bovensmann, J., Frerick, J., and Burrows, J.: Measurements of molecular

absorption spectra with the SCIAMACHY pre-flight model: instrument characterization and

reference data for atmospheric remote sensing in the 230-2380 nm region, J. Photochemistry and

Photobiology A: Chemistry, Vol 157, No. 2-3, 167-184, 2003.

Boughner R. E., Larsen, J. E., and Natarajan., M.: The influence of NO and ClO variations at

twilight on the interpretation of solar occultation measurements, Geophys. Res. Lett., 7, 231 –

234, 1980.

Brohede, S. M., Haley, C. S., McLinden, C. A., Sioris, C. E., Murtagh, D. P., Petelina, S. V.,

Llewellyn, E. J., Bazureau, A., Goutail, F., Randall, C. E., Lumpe, J. D., Taha, G., Thomasson,

L. W., and Gordley, L. L.: Validation of Odin/OSIRIS stratospheric NO_2 profiles, J. Geophys.

Res.-Atmos., 112, D07310, https://doi.org/10.1029/2006JD007586, 2007.

Brühl, C., Drayson, S. R., Russell III, J. M., Crutzen, P. J., McInerney, J. M., Purcell, P. N.,

Claude, H., Gernandt, H., McGee, T. J., McDermid, I. S., and Gunson, M. R.: Halogen

Occultation Experiment ozone channel validation, J. Geophys. Res., Vol. 101, NO. D6, 10,217 -

10,240, 1996.

Byrne, G. D., and Hindmarsh, A. C.: A polyalgorithm for the numerical solution of ordinary

differential equations, ACM Trans. Math. Soft., 1(1), 71-96, 1975.

Callis, L. B., Natarajan, M., Lambeth, J. D., and Boughner, R. E.: On the origin of midlatitude

ozone changes: Data analysis and simulations for 1979 – 1993, J.Geophys. Res., 102, 1215 –

1228, 1997.

536   Connor, B. J., Siskind, D. E., Tsou, J. J., Parrish, A., and Remsberg, E. E.: Ground-based

537   microwave observations of ozone in the upper stratosphere and mesosphere, J. Geophys. Res.,

538   vol 99, No. D8, 16,757-16,770, 1994.

539   Dubé, K., Bourassa, A., Zawada, D., Degenstein, D., Damadeo, R., Flittner, D., and Randel, W.:

540   Accounting for the photochemical variation in stratospheric NO_2 in the SAGE III/ISS solar

541   occultation retrieval, Atmos. Meas. Tech., 14, 557 – 566, https://doi.org/10.5194/amt-14-557-

542   2021, 2021.

543   Gordley, L. L., Russell III, J. M., Mickley, L. J., Frederick, J. E., Park, J. H., Stone, K. A.,

544   Beavee, G. M., McInerney, J. M., Deaver, L. E., Toon, G. C., Murcray, F. J.,Blatherwick, R. D.,

545   Gunson, M. R., Abbatt, J. P. D., Mauldin III, R. L., Mount, G. H., Sen, B., and Blavier, J. F.:

546   Validation of nitric oxide and nitrogen dioxide measurements made by the Halogen Occultation

547   Experiment for UARS platform, J. Geophys. Res.-Atmos., 101,10241–10266, 1996.

548   JPL Publication 19-5, Chemical Kinetics and Photochemical Data for Use in Atmospheric

549   Studies, Evaluation Number 19. https://jpldataeval.jpl.nasa.gov/pdf/NASA-

550   JPL%20Evaluation%2019-5.pdf, 2020.

551   Livesey, N. J., Read, W. G., Wagner, P. A., Froidevaux, L., Santee, M. L., Schwartz, M. J.,

552   Lambert, A., Millan Valle, L. F., Pumphrey, H. C., Manney, G. L., Fuller, R. A., Jarnot, R. F.,

553   Knosp, B. W., and Lay, R. R.: Earth Observing System (EOS) Aura Microwave Limb Sounder

554   (MLS) Version 5.0x Level 2 and 3 data quality and description document, JPL D-105336 Rev B,

555   2022.

556   McCormick, M. P., Lei, L., Hill, M. T., Anderson, J., Querel, R., and Steinbrecht, W.: Early

557   results and validation of SAGE III-ISS ozone profile measurements from onboard the

558   International Space Station, Atmos. Meas. Tech., 13, 1287-1297, https://doi.org/10.5194/amt-13-

559   1287-2020, 2020.

560   Natarajan, M., Deaver, L. E., Thompson, E., and Magill, B.: Impact of twilight gradients on the

561   retrieval of mesospheric ozone from HALOE, J. Geophys. Res., Vol. 110,

562   doi:10.1029/2004JD005719, 2005.

563   Newchurch, M. J., Allen, M., Gunson, M. R., Salawitch, R. J., Collins, G. B., Huston, K. H.,

564   Abbas, M. M., Abrams, M. C., Chang, A. Y., Fahey, D. W., Gao, R. S., Irion, F. W.,

565   Loewenstein, M., Manney, G. L., Michelson, H. A., Podolske, J. R., Rinsland, C. P., and Zander,

566   R.: Stratospheric NO and NO_2 abundances from ATMOS Solar-Occultation Measurements,

567   Geophys. Res. Lett., 23, 2373-2376., https://doi.org/10.1029/96GL01196,1996.

568   Parrish, A., Boyd, I. S., Nedoluha, G. E., Bhartia, P. K., Firth, S. M., Kramarova, N. A., Connor,

569   B. J., Bodeker, G. E., Froidevaux, L., Shiotani, M., and Sakazaki, T.: Diurnal variations of

570   stratospheric ozone measured by ground-based microwave remote sensing at the Mauna Loa

571   NDACC site: measurement validation and GEOSCCM model comparison, Atmos. Chem. Phys.,

572   14, 7255-7222, www.atmos-chem-phys.net/14/7255/2014/doi:10.5194/acp-14-7255-2014, 2014

573   Remsberg, E., Damadeo, R., Natarajan, M., and Bhatt, P.: Observed responses of mesospheric

574   water vapor to solar cycle and dynamical forcings, J. Geophys. Res., 123 (7), 3830-3843,

575   https://doi.org/10.1002/2017JD028029, 2018.

576   Russell III, J. M., Farmer, C. B., Rinsland, C. P., Zander, R., Froidevaux, L., Toon, G. C., Gai,

577   B., Shaw, J., and Gunson, M.: Measurements of Odd Nitrogen Compounds in the Stratosphere

578   by the ATMOS Experiment on Spacelab 3, J. Geophys. Res., Vol 3, D2, 1718-1736, 1988.

579   Sauvageat, E., Barras, E. M., Hocke, K., Haefele, A., and Murk, A.: Harmonized retrieval of

580   middle atmospheric ozone from two microwave radiometers in Switzerland,

581   https://doi.org/10.5194/amt-2022-212, 2022

582   SAGE III Algorithm Theoretical Basis Document (ATBD) Solar and Lunar Algorithm, LaRC

583   475-00-109, Version 2.1. https://eospso.gsfc.nasa.gov/sites/default/files/atbd/atbd-sage-solar-

584   lunar.pdf, 2002

585   SAGE III/ISS Data Products User's Guide, Version 3.0,

586   https://asdc.larc.nasa.gov/documents/sageiii-iss/guide/DPUG-G3B-2-0.pdf, 2021.

587   Strode, S. A., Taha, G., Oman, L. D., Damadeo, R., Flittner, D., Schoeberl, M., Sioris, C. E., and

588   Stauffer, R.: SAGE III/ISS ozone and NO_2 validation using diurnal scaling factors,

589   https://doi.org/10.5194/amt-15-6145-2022, Atmos. Meas. Tech., 15, 6145-6161, 2022

590   Wang, H. J. R., Damadeo, R., Flittner, D., Kramarova, N., Taha, G., Davis, S., et al.: Validation

591   of SAGE III/ISS solar occultation ozone products with correlative satellite and ground-based

592   measurements, J. Geophys. Res., 125, e2020JD032430. https://doi.org/10.1029/2020JD032430,

593   2020.

594   Yue, J., Russell III, J., Gan, Q., Wang, T., Rong, P., Garcia, R., and Mlynczak, M.:Increasing

595   water vapor in the stratosphere and mesosphere after 2002, Geophys. Res. Lett., 46, 13,452-

596   13,460. https://doi.org/10.1029/2019GL084973, 2019.

597

598
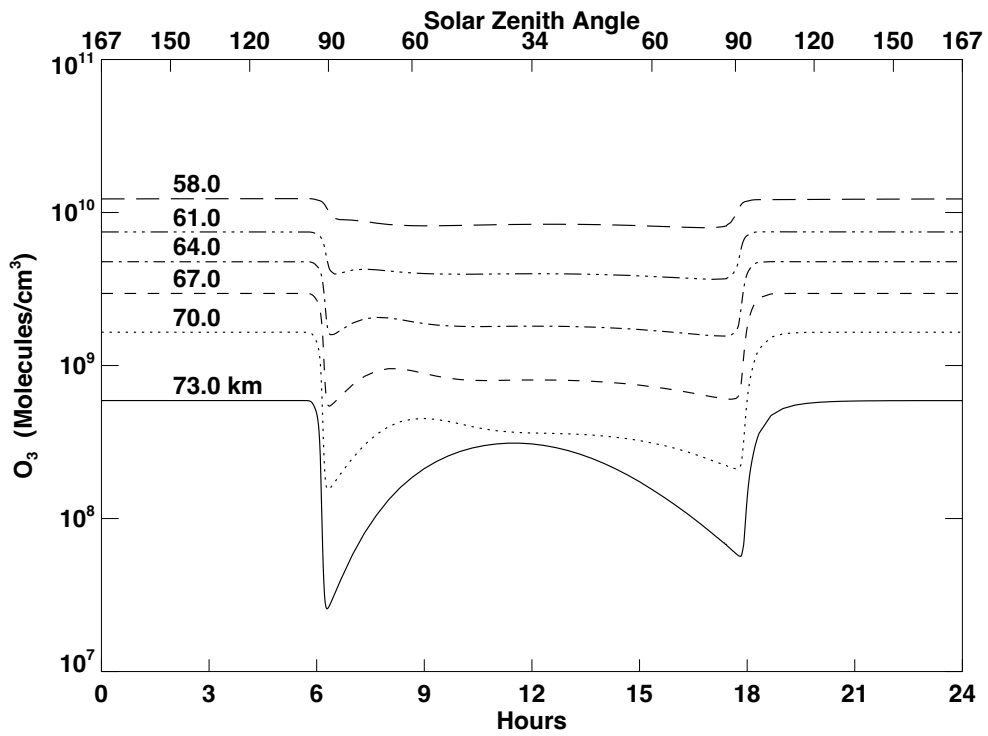
599

600   Figure 1. Diurnal variation in O_3 at 11.25° S in June at altitudes from 58 to 73 km. 0 hours

601   denote midnight. The upper X axis shows the variation of SZA.

Solar Occultation Geometry
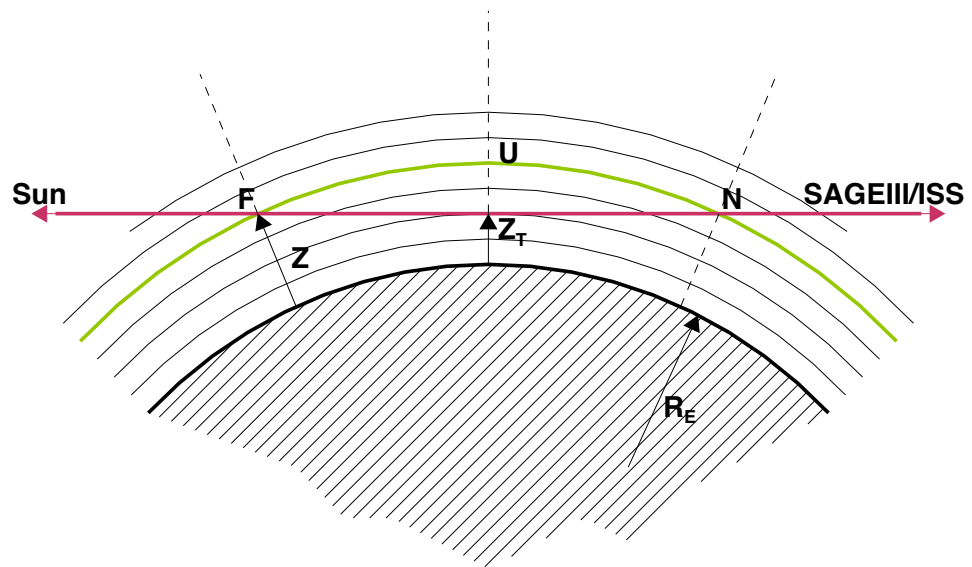
Z_T Tangent altitude, Z Altitude of a layer above the tangent path

R_E Earth radius

602

603   Figure 2. Schematic representation of the solar occultation measurement. Z_T is the tangent

604   altitude, red line is the LOS, Z is the altitude of a layer above the tangent altitude, F (towards

605   sun) and N (towards SAGE III/ISS) are the points of intersection of layer at Z with the LOS, and

606   R_E is the earth radius.

607

Sunrise, 64 (km)   11.25° S JUN
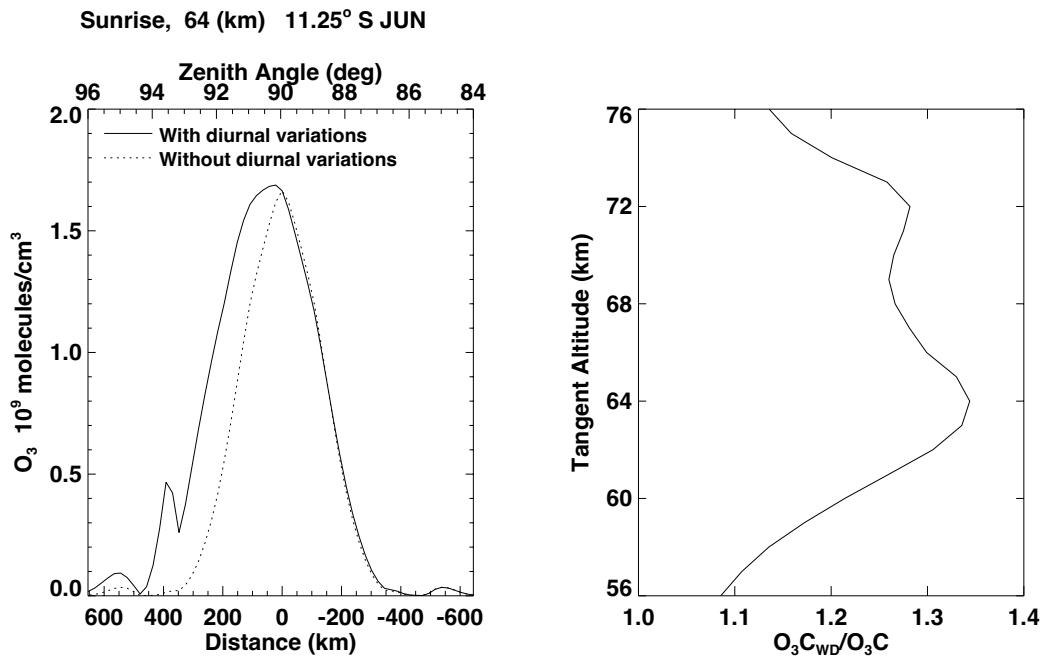
608

609   Figure 3. (Left) O_3 concentration along the LOS for a tangent altitude of 64 km at sunrise at

610   11.25° S latitude in June. Solid line shows O_3 with diurnal variations and the dotted line

611   represents O_3 without diurnal variations. The X-axis represents the distance along the LOS

612   relative to the tangent point with positive direction towards the instrument and negative direction

613   towards the Sun. The upper axis shows the corresponding SZA. (Right) Ratio of the O_3 column

614   along the LOS with appropriate diurnal variations to the O_3 column without diurnal variations,

615   plotted as a function of altitude at 11.25° S in June.

616

617

618

Sunrise O$_3$ twilight ratio JUN 11.25° S
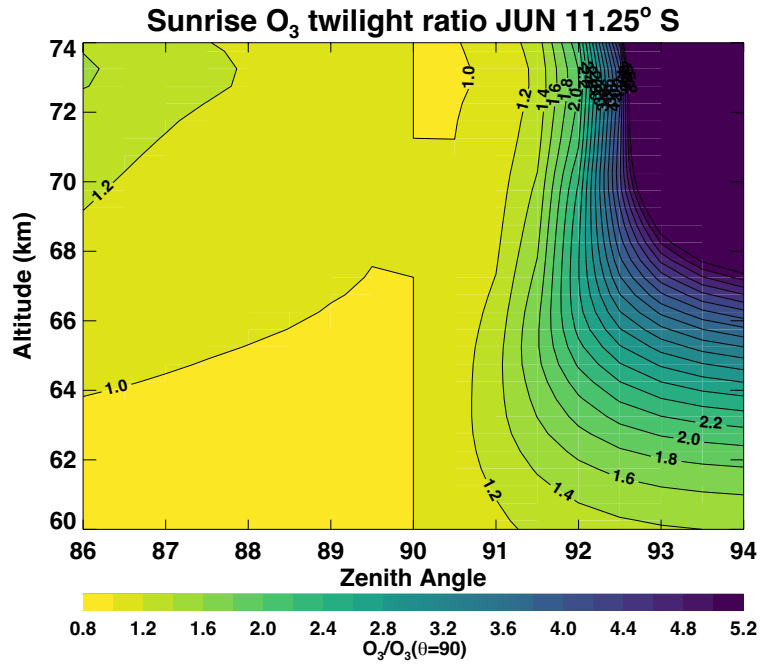
619

620   Figure 4. Ozone twilight ratio, defined as O$_3$ at solar zenith angle θ/O$_3$ at θ=90°, as a function

621   of SZA and altitude for sunrise in June and 11.25° S latitude.
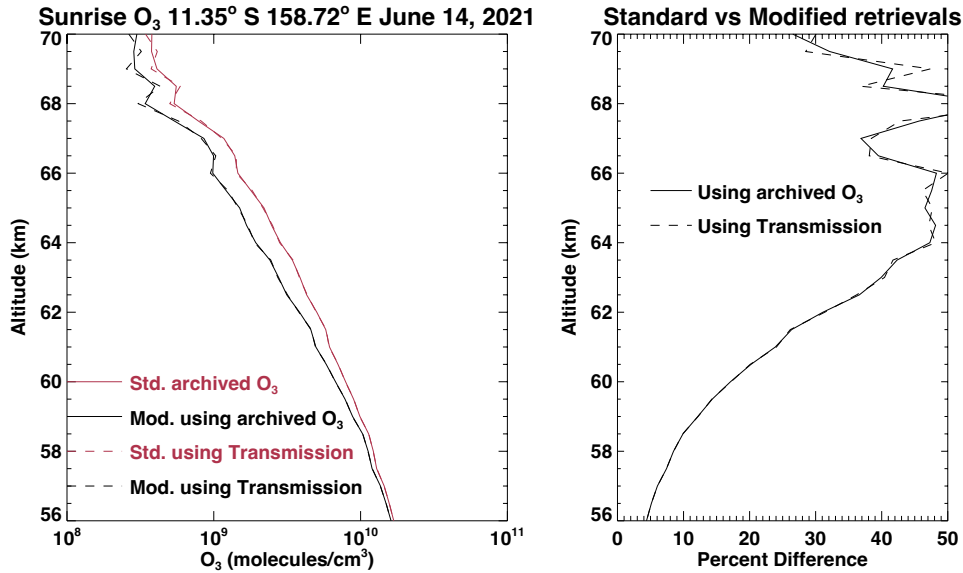
622

623

Sunset O$_3$ twilight ratio JUN 11.25° S
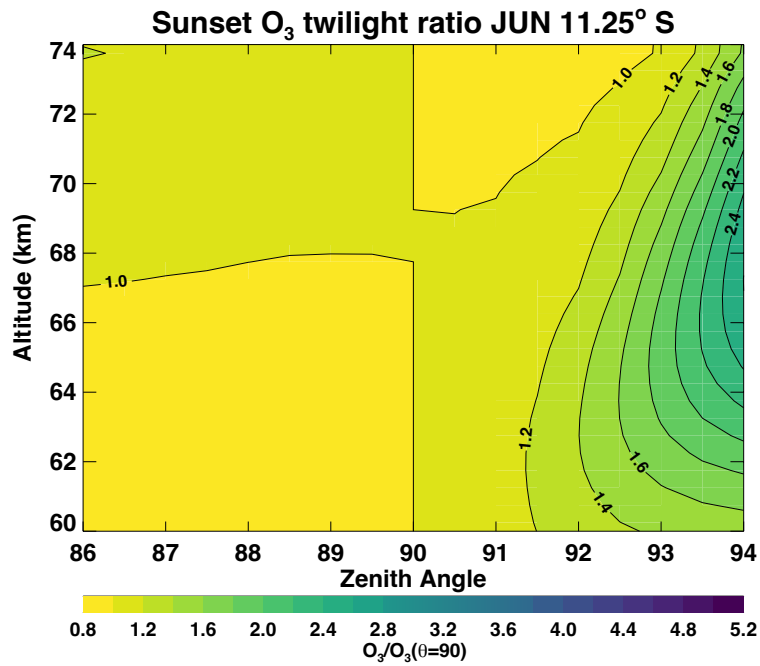
624

625   Figure 5. Ozone twilight ratio, defined as O$_3$ at solar zenith angle θ/O$_3$ at θ=90°, as a function

626   of SZA and altitude for sunset in June and 11.25° S latitude.

627
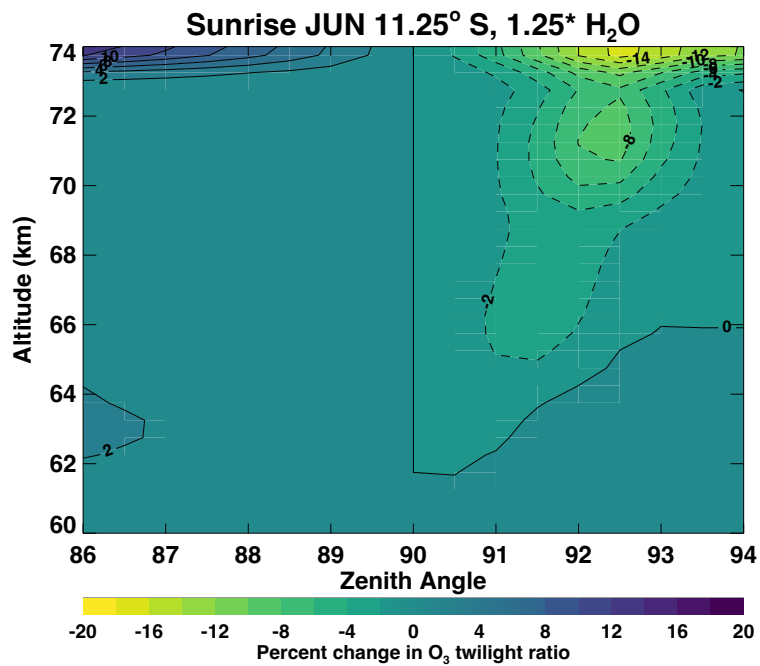
Figure 6. Percent change in the O_3 twilight ratio shown in Fig.4 when the H_2O in the diurnal model is increased by 25% at all altitudes. This figure corresponds to sunrise at 11.25° S in June.

Sunrise O$_3$ 11.35^o S 158.72^o E June 14, 2021 **Standard vs Modified retrievals**

Std. archived O$_3$

Mod. using archived O$_3$

Std. using Transmission

Mod. using Transmission

Using archived O$_3$

Using Transmission

Altitude (km)

O$_3$ (molecules/cm^3)

Percent Difference

631

Figure 7. SAGE III/ISS O$_3$ for a sunrise event at 11.35° S and 158.72° E on June 14, 2021

(Event ID 2021061438SR). (Left panel) Red solid line shows the standard SAGE III retrieval,

and the black solid line represents the retrieval including the diurnal variations along LOS. The

dashed lines represent the retrievals using the transmission data, the red color for the standard

retrieval and the black denoting the retrieval with diurnal corrections. (Right panel) Percent

difference between the standard retrieval and the one with diurnal corrections; solid line using

the archived standard retrieval of O$_3$ concentration, and the dashed line based on the approximate

retrieval using the transmission data.

640

Sunset O$_3$ 12.05^o S 151.16^o E June 15, 2021

Standard vs Modified retrievals
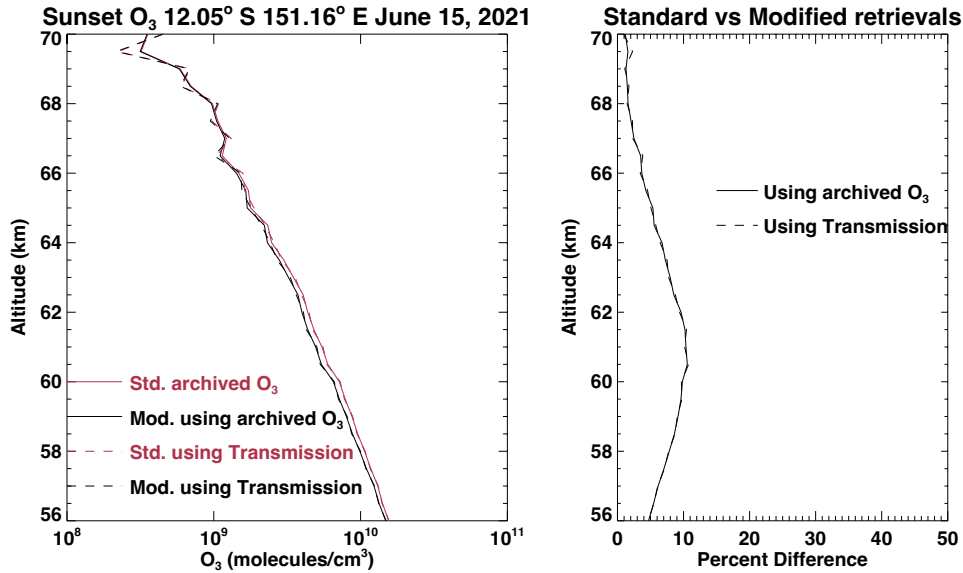
641

642   Figure 8. SAGE III/ISS O$_3$ for a sunset event at 12.05° S and 151.16° E on June 15, 2021 (Event

643   ID 2021061515SS). (Left panel) Red solid line shows the standard SAGE III retrieval, and the

644   black solid line represents the retrieval including the diurnal variations along LOS. The dashed

645   lines represent the retrievals using the transmission data, the red color for the standard retrieval

646   and the black denoting the retrieval with diurnal corrections. (Right panel) Percent difference

647   between the standard retrieval and the one with diurnal corrections; solid line using the archived

648   standard retrieval of O$_3$ concentration, and the dashed line based on the approximate retrieval

649   using the transmission data.

650

35

Sunrise O₃ Standard vs Modified retrievals, JUN 2021
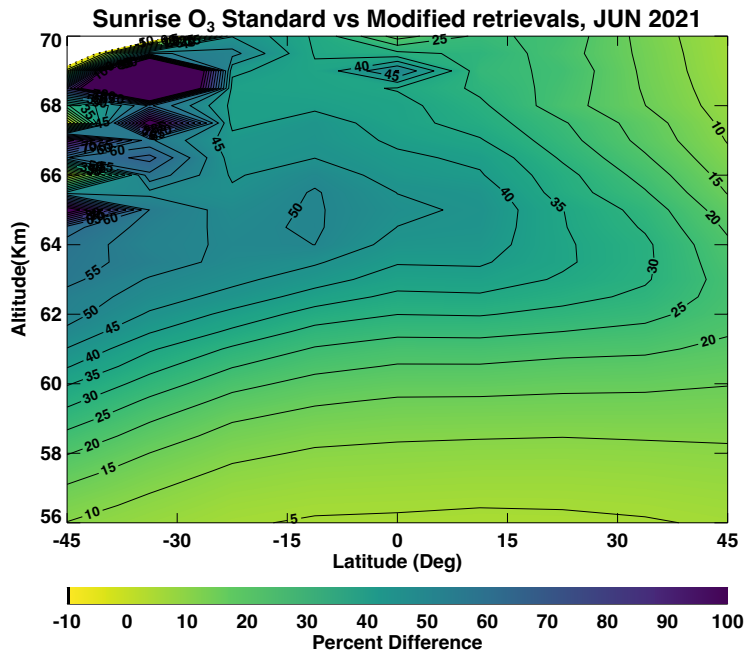
651

652   Figure 9. Latitudinal average of the percent difference in sunrise O_3 between the standard

653   (archived) retrieval and a retrieval including diurnal variations along the LOS, as a function of
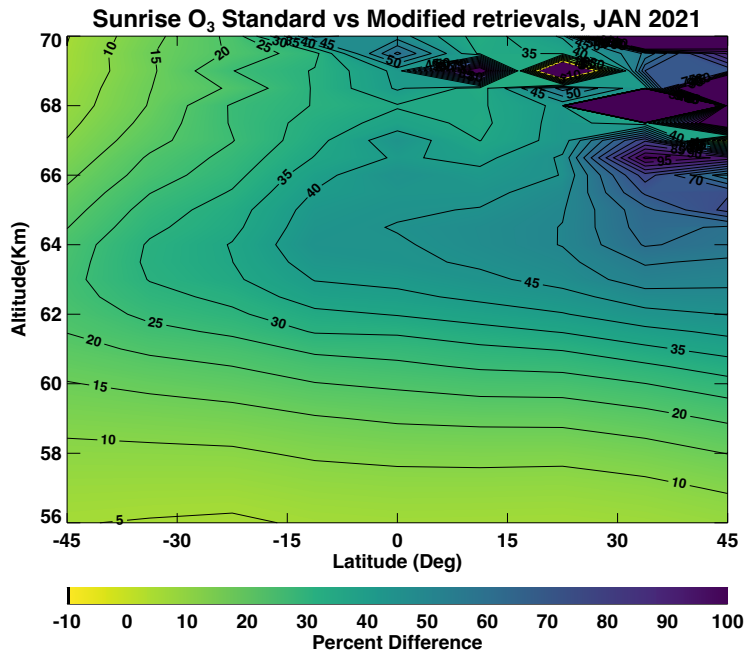
654   latitude and altitude for June 2021.

655

656

Sunset O$_3$ Standard vs Modified retrievals, JUN 2021
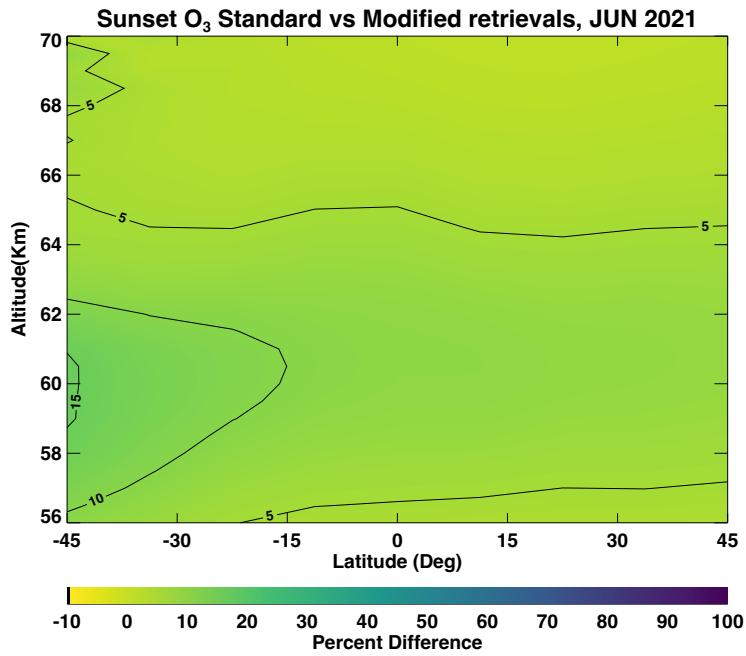
657

658   Figure 10. Latitudinal average of the percent difference in sunset O$_3$ between the standard

659   (archived) retrieval and a retrieval including diurnal variations along the LOS, as a function of

660   latitude and altitude for June 2021.

Figure 11. Latitudinal average of the percent difference in sunrise O_3 between the standard
(archived) retrieval and a retrieval including diurnal variations along the LOS, as a function of
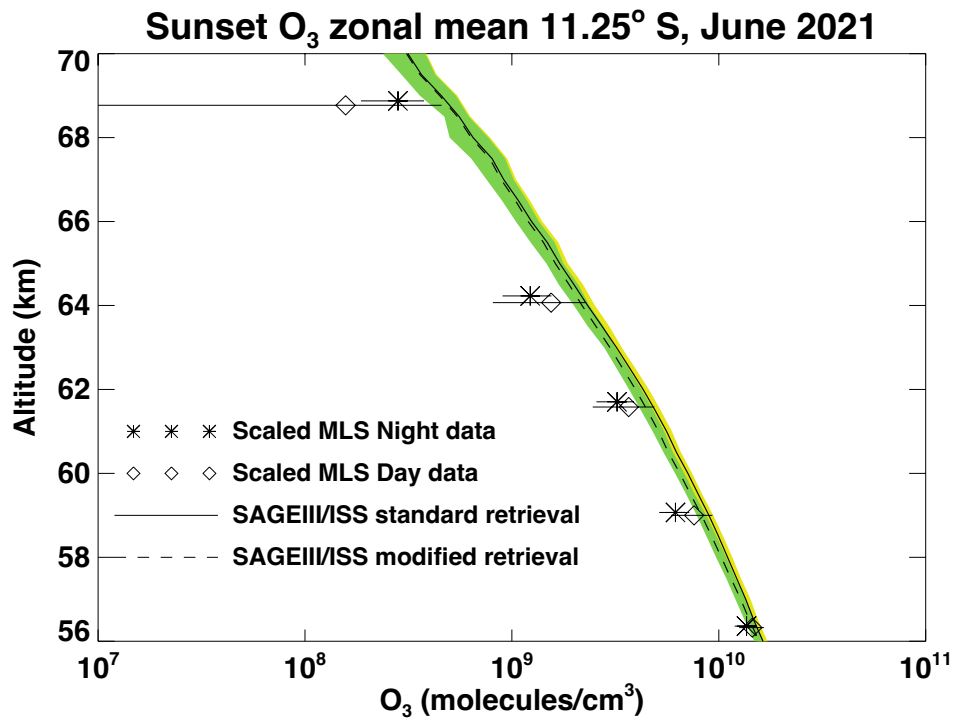latitude and altitude for January 2021.
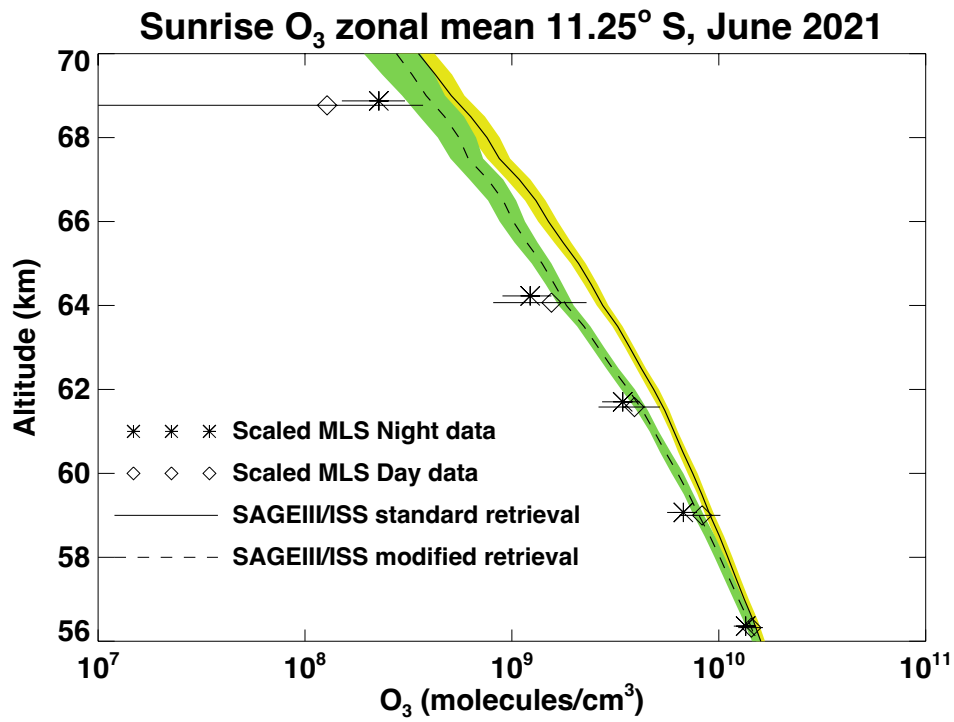
Figure 12. Comparison of sunrise SAGE III/ISS and MLS mesospheric O_3 zonal mean at
11.25° S in June 2021. Solid line – mean of SAGE III/ISS standard retrieval with the standard
deviation shown by the yellow shade; Dashed line – mean of SAGE III/ISS modified retrieval
with the standard deviation shown by the green shade; Asterisks – mean MLS night data scaled
to sunrise; Diamonds – mean MLS day data scaled to sunrise; Horizontal lines represent the
standard deviations.

667

668

669

670

671

672

673

674

**Sunset O$_3$ zonal mean 11.25^o S, June 2021**

675

676   Figure 13. Comparison of sunset SAGE III/ISS and MLS mesospheric O$_3$ zonal mean at

677   11.25° S in June 2021. Solid line – mean of SAGE III/ISS standard retrieval with the standard

678   deviation shown by the yellow shade; Dashed line – mean of SAGE III/ISS modified retrieval

679   with the standard deviation shown by the green shade; Asterisks – mean MLS night data scaled

680   to sunset; Diamonds – mean MLS day data scaled to sunset; Horizontal lines represent the

681   standard deviations.

682

SAGEIII/ISS Jun 2021
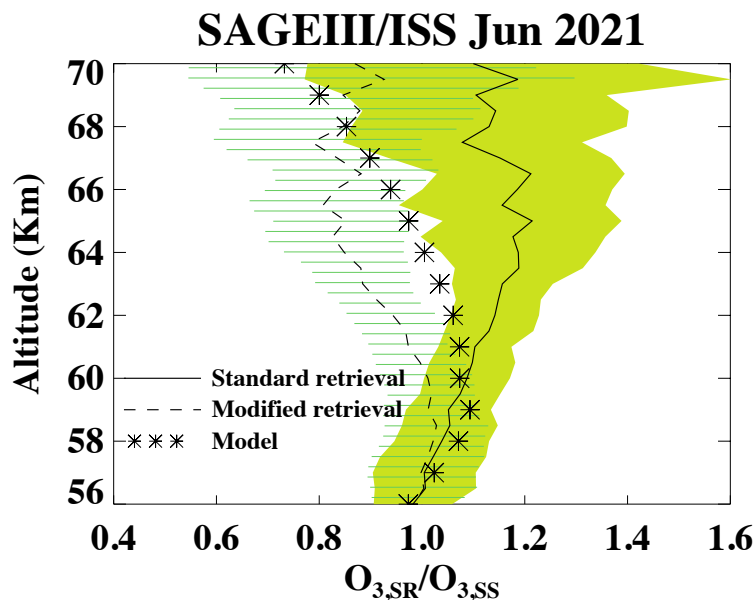
683

684   Figure 14. Vertical profile of O_3 sunrise to sunset ratio in June 2021. Nearly collocated 10 pairs

685   of sunrises (mean latitude 10.46° S) and sunsets (mean latitude 10.27° S) data are used for this

686   plot. Solid line shows the mean ratio from standard (archived) retrieval and the green shade

687   represents the standard deviation; Dashed line shows the mean ratio from the retrieval including

688   diurnal variations along the LOS and the horizontal lines represent the standard deviation. The

689   asterisk symbols are the ratios from diurnal photochemical calculations at 11.25° S for June.